Propagation of whistler mode chorus to low altitudes: Spacecraft observations of structured ELF hiss

Ondřej Santolík, J. Chum, Michel Parrot, D.A. Gurnett, J.S. Pickett, Nicole Cornilleau-Wehrlin

Propagation of whistler mode chorus to low altitudes: Spacecraft observations of structured ELF hiss

O. Santolík,[1,2] J. Chum,[3] M. Parrot,[4] D. A. Gurnett,[1] J. S. Pickett,[1] and N. Cornilleau-Wehrlin[5]

[1]   We interpret observations of low-altitude electromagnetic ELF hiss observed on the dayside at subauroral latitudes. A divergent propagation pattern has been reported between 50° and 75° of geomagnetic latitude. The waves propagate with downward directed wave vectors which are slightly equatorward inclined at lower magnetic latitudes and slightly poleward inclined at higher latitudes. Reverse ray tracing using different plasma density models indicates a possible source region near the geomagnetic equator at a radial distance between 5 and 7 Earth radii by a mechanism acting on highly oblique wave vectors near the local Gendrin angle. We analyze waveforms received at altitudes of 700–1200 km by the Freja and DEMETER spacecraft and we find that low-altitude ELF hiss contains discrete time-frequency structures resembling wave packets of whistler mode chorus. Emissions of chorus also predominantly occur on the dawnside and dayside and have recently been considered as a possible source of highly accelerated electrons in the outer Van Allen radiation belt. Detailed measurements of the Cluster spacecraft at radial distances of 4–5 Earth radii show chorus propagating downward from the source region localized close to the equator. The time-frequency structure and frequencies of chorus observed by Cluster along the reverse raypaths of ELF hiss are consistent with the hypothesis that the frequently observed dayside ELF hiss is just the low-altitude manifestation of natural magnetospheric emissions of whistler mode chorus.

1.   Introduction

[2]   Extremely low frequency (ELF) hiss is a broadband electromagnetic emission in the frequency range from a few hundred Hz up to about 2 kHz. It has been commonly observed for more than 4 decades. The early ground-based [*Aarons et al.*, 1960; *Laaspere et al.*, 1964] and low-altitude (several hundreds to a thousand kilometers) satellite observations [*Gurnett and O'Brien*, 1964; *Taylor and Gurnett*, 1968] revealed that ELF hiss predominantly occurs on the dayside and at high geomagnetic latitudes (between about 50° and 75°). These results have been later confirmed by a number of spacecraft observations at low altitudes [e.g., *Barrington et al.*, 1971; *Parrot*, 1990; *Rauch et al.*, 1993].

[3]   These results seem to contradict the early observations reported from the spacecraft orbiting at high altitudes

of a few Earth radii. *Russell et al.* [1969] and *Thorne et al.* [1973] concluded that steady hiss could be found almost everywhere in the plasmasphere, independently of the local time, referring to this type of emission as plasmaspheric hiss. At high latitudes outside the plasmasphere, however, similar measurements also revealed a frequent dayside occurrence, consistent with the observations at low altitudes [e.g., *Gurnett and O'Brien*, 1964]. The low-altitude ELF hiss thus should not be confused with the plasmaspheric hiss. The two types of emissions have remarkably different occurrence patterns. Plasmaspheric hiss also stays enclosed in the plasmasphere and never penetrates to low altitudes or to the ground. *Solomon et al.* [1988] and *Cornilleau-Wehrlin et al.* [1993] studied plasmaspheric hiss with GEOS-1 wave and electron data. They concluded that plasmaspheric hiss can be generated by anisotropic electron distribution function by cyclotron resonance and that the observed intensity level can be reached in a single pass through the equatorial region. The occurrence patterns of plasmaspheric hiss have been recently studied by *Green et al.* [2005] who, based on results of their wave-mapping technique, related this emission to lightning induced whistlers.

[4]   On the other hand, the occurrence pattern of low-altitude ELF hiss strongly resembles known properties of the whistler mode chorus emissions. Chorus was also first

---

[1]Department of Physics and Astronomy, University of Iowa, Iowa City, Iowa, USA.
[2]Permanently at Faculty of Mathematics and Physics, Charles University, Prague and IAP/CAS, Prague, Czech Republic.
[3]Institute of Atmospheric Physics, CAS, Prague, Czech Republic.
[4]LPCE/CNRS, Orléans, France.
[5]CETP/IPSL, Vélizy, France.

observed on the ground [*Storey*, 1953] as "dawn chorus," and later spacecraft measurements confirmed its predominant occurrence during the local morning and day time [e.g., *Burtis and Helliwell*, 1976; *Koons and Roeder*, 1990]. Earthward drifting electrons from the magnetospheric tail are believed to be the source population for chorus. In the Earth's magnetic field, their drift is directed toward the local morning and day side. Here they interact with whistler mode waves, often generating discrete wave packets which change their frequency at timescales of a fraction of a second. A yet not fully understood nonlinear amplification mechanism based on the electron cyclotron resonance [e.g., *Trakhtengerts*, 1999; *Nunn et al.*, 1997] takes place close to the equatorial plane [*Helliwell*, 1967; *LeDocq et al.*, 1998; *Lauben et al.*, 2002; *Santolík et al.*, 2005]. After its generation chorus can propagate as an unducted emission [*Lauben et al.*, 2002; *Santolík et al.*, 2003a; *Parrot et al.*, 2004a], and it has been shown to undergo magnetospheric reflection and degradation of its discrete structure into hiss [*Parrot et al.*, 2004b]. Whistler mode chorus has recently received an increased attention since it might be considered as a possible source of highly accelerated electrons in the outer Van Allen radiation belt [*Meredith et al.*, 2001, 2003; *Horne et al.*, 2003]. Ground-based observations of chorus play a significant role in these investigations [e.g., *Horne et al.*, 2005, and references therein]. Since chorus and the low-altitude ELF hiss have similar local time distribution and also a similar frequency range, it would be interesting to examine their possible relation. This is the main aim of the present paper.

[5] Low-altitude ELF hiss is often characterized by a lower-frequency cutoff occurring just below the local hydrogen cyclotron frequency (f_{H^+}). *Gurnett and Burns* [1968] identified this abrupt step in wave spectra with the local multiion cutoff acting on downward propagating waves. Sometimes, broadband electromagnetic waves occur also at much lower frequencies below f_{H^+}, especially at subauroral latitudes [*Santolík and Parrot*, 1998]. These waves propagate with wave vectors very close to the direction of the Earth's magnetic field ($\mathbf{B_0}$). They most probably penetrate to these frequencies by tunnelling of the right-hand circularly polarized ELF hiss below the multiion crossover frequency and are thus not affected by the multiion cutoff of the left-hand polarized mode. The occurrence pattern of these waves is also very similar to that of ELF hiss [*Santolík and Parrot*, 1998].

[6] The upper-frequency limit of low-altitude ELF hiss is rather diffuse at higher latitudes, and fluctuates around a few kHz. The upper cutoff usually becomes sharp and stable at magnetic latitudes below about 55°, the latitude of which roughly corresponds to the projection of plasmapause to low-altitudes. Although low-altitude ELF hiss with a sharply defined upper frequency limit was already found by *Gurnett and O'Brien* [1964], this phenomenon was first studied in detail by *Muzzio and Angerami* [1972]. The band limitation has been explained by the effects of propagation from the source region, supposing that waves are generated at a large angle θ, where θ is the angle between the wave vector ($\mathbf{k}$) and the ambient magnetic field ($\mathbf{B_0}$).

[7] Key information on the hiss origin has been obtained by wave propagation studies. First results were obtained by *Mosier and Gurnett* [1969] and *Mosier* [1971]. Using simultaneous measurements of electric and magnetic antennae, they systematically estimated whether the waves propagate upward or downward. ELF hiss was found to propagate downward over the entire range of magnetic latitudes under study (35° to 75°), whereas upgoing hiss was only observed at latitudes below about 60°. These results are explained by reflection of waves propagating originally outside the plasmasphere downward at low θ. *Mosier* [1971] proposed a reflection mechanism at the plasmapause density gradient, where the wave vector becomes nearly perpendicular to $\mathbf{B_0}$ (θ near 90°). At some height the wave reflects due to the altitude variation of the perpendicular refractive index. The minimum reflection height was estimated from 1500 km to above 3000 km at the dayside and below 1000 km at the nightside.

[8] *Lefeuvre et al.* [1992] presented a thorough analysis of the ELF hiss propagation at low altitudes (≈1000 km) for three typical cases. At high latitudes outside the plasmasphere, they found intense downgoing waves at low θ. Within the plasmapause density gradient, the hiss is upgoing and propagates equatorward at high θ. This led the authors to suggest that the source of ELF hiss lies at high altitudes in the diffuse auroral region. The waves are reflected below the satellite orbit and directed upward to the plasmasphere. Simultaneous observation of downgoing and reflected upgoing waves in the vicinity of the local f_{H^+} is reported. Reflection at the local multiion cutoff frequency, as first proposed by *Gurnett and Burns* [1968], is believed to be a very efficient process but *Lefeuvre et al.* [1992] propose also possible reflection at the ionospheric layers.

[9] Similar findings about the ELF hiss propagation at low altitudes have been presented by *Rauch et al.* [1985], *Hayakawa et al.* [1985], and *Rauch et al.* [1993]. *Santolík and Parrot* [1999] have proposed to explain the band-limitation of hiss at lower latitudes by the height dependence of the reflection coefficient below the satellite altitude (1500–1700 km). They have also indicated the divergence of wave vector directions at both latitudinal edges of the hiss emission and subsequent reflection: equatorward at lower latitudes and poleward at high latitudes. This propagation pattern, together with reflection of poleward propagating hiss has been studied in detail by *Santolík and Parrot* [2000] using various analysis techniques. Wave distribution function (WDF) analysis has shown simultaneous propagation of both originally downgoing and poleward reflected upgoing waves.

[10] In the present paper we provide a geophysical interpretation of the observed divergent propagation pattern of low-altitude ELF hiss, and we put these commonly observed wave emissions into a broader context. We use backward ray tracing techniques based on the wave-normal directions measured at low altitudes. Following the waves toward their anticipated source region, we find that they may originate near the equator well above the average position of the plasmapause. This region is consistent with the source region of whistler mode chorus. This fact and also the remarkable similarity of the reported morningside and dayside occurrence of chorus and low-altitude ELF hiss lead us to the hypothesis that ELF hiss is nothing else than chorus propagating to low altitudes. Examining in detail the data recorded by the Freja spacecraft and also by the recently launched DEMETER spacecraft, we find discrete
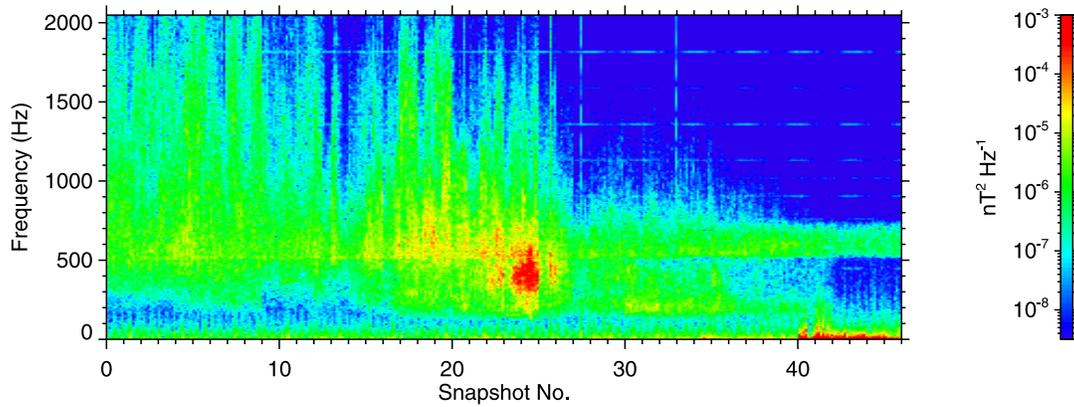
Figure 1. Time-frequency power spectrogram of the B_y component of magnetic field fluctuations measured by Freja on 8 April 1995. The horizontal axis is annotated by snapshot numbers (see text) and covers a time interval from 1549:53 UT to 1555:56 UT. The corresponding portion of the spacecraft orbit is located in the morning sector (0600 to 0810 MLT) at geomagnetic latitudes between 56° and 71°, and at altitudes between 1000 and 1200 km.

time-frequency structures resembling the chorus wave packets in both data sets. Indeed, chorus recorded at high altitudes by the Cluster spacecraft appears in the same frequency range close to the positions of reverse rays obtained from the low-altitude observations. These measurements are thus also consistent with propagation of chorus to low altitudes. *Chum and Santolík* [2005] studied the propagation pattern of nonducted whistler mode chorus using the direct ray tracing simulation from a source region located close to the equatorial plane. They found that the waves which leave the source with wave vectors highly inclined from $\mathbf{B_0}$ toward the Earth can reach the topside ionosphere. This is consistent with the results of the present paper.

[11] In the next section we describe the observed propagation properties of the low-altitude ELF hiss. Section 3 presents the results of the backward ray tracing analysis. Section 4 shows detailed analysis of the time-frequency structure of low-altitude ELF hiss recorded by the Freja and DEMETER spacecraft and comparison with high-altitude measurements of the Cluster spacecraft. Finally, section 5 presents a brief discussion and conclusions.

## 2. Results of Propagation Analysis of Low-Altitude ELF Hiss

[12] *Santolík and Parrot* [2000] presented analysis of measurements of the Freja spacecraft on 8 April 1995. The main aim of that paper was to compare different methods for estimating the wave distribution function and wave vector directions. The analysis was based on the data of the F4 wave experiment [*Holback et al.*, 1994]. In its normal mode of operation in the lowest-frequency band the instrument simultaneously recorded waveforms of three orthogonal components of the magnetic field fluctuations and one component of the electric field fluctuations, with a sampling frequency of 4096 Hz. On 8 April 1995, the instrument was programmed to record cyclic measurements of data snapshots with the duration of 3 s repeated every 8 s.

[13] Figure 1 shows an overview frequency-time power spectrogram of the B_y component of magnetic field fluctua-

tions (B_y is perpendicular to the static magnetic field and to the plane of the local magnetic meridian). Every data snapshot is processed separately and the snapshot number is given on the horizontal axis. The first snapshot starts at 1549:53 UT and the last snapshot ends at 1555:56 UT. During that time the spacecraft moves at geomagnetic latitudes from 56° to 71°, at altitudes between 1000 and 1200 km, and the magnetic local time (MLT) runs from 0600 to 0810 MLT. The spectrogram shows an emission of low altitude ELF hiss in the morning sector at subauroral latitudes. A multiion cutoff described by *Gurnett and Burns* [1968] appears in the spectra just below the local proton cyclotron frequency (f_{H^+}) which is between 500 and 540 Hz in this time interval. With an exception of a narrow frequency interval between this cutoff and f_{H^+}, analysis of *Santolík and Parrot* [2000] showed that the waves are right-hand polarized and correspond thus to the magnetosonic-whistler cold plasma mode. This mode identification was further confirmed by comparing the measurements with the magnetic and electric field components calculated from the cold plasma theory. This comparison was an integral part of the estimation of the wave distribution function in selected points of the time-frequency plane [*Santolík and Parrot*, 2000].

[14] Analysis of the direction of Poynting flux and of the wave normal directions [*Santolík and Parrot*, 2000] showed that the waves predominantly propagate from higher altitudes toward the Earth. The results of this analysis are, for two frequency intervals, illustrated in Figure 2. The frequency interval 620–640 Hz (Figure 2a) demonstrates a divergent propagation pattern of downward propagating waves at lower latitudes. Upward and poleward obliquely propagating waves are observed at magnetic latitudes above 70°. These waves correspond to the band-limited emission observed between 500 and 750 Hz after 1555 UT, seen on Figure 1 starting by snapshot 38.

[15] Results for a higher frequency interval between 780 and 820 Hz (Figure 2b) do not show any upward propagating waves. However, the diverging and downward propagating waves have very similar evolution of wave vector directions in both frequency bands. The wave vectors are
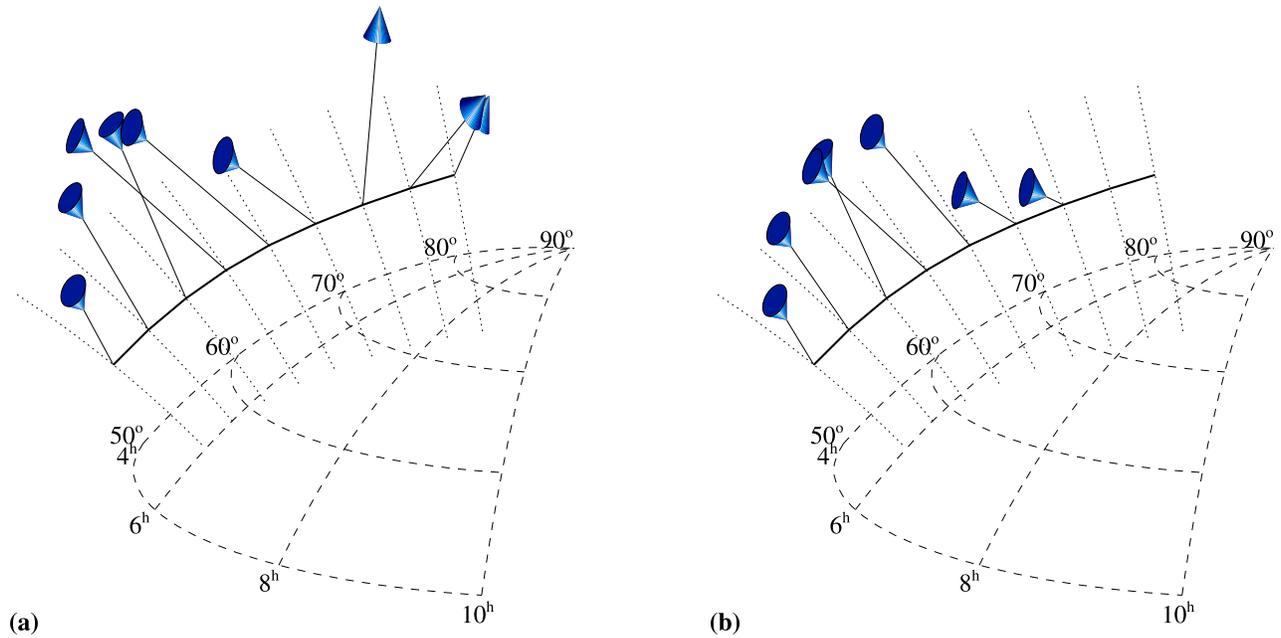
Figure 2. Observed wave-normal directions along the orbit of the Freja spacecraft on 8 April 1995. Dashed lines: magnetic parallels and meridians on the Earth surface labeled respectively by their magnetic latitude and MLT. Thick line: a part of the spacecraft orbit between 1549 and 1557 UT. Dotted lines: magnetic field lines at the spacecraft position calculated with a time resolution of one minute. Thin solid lines with shaded arrows: measured wave vector directions averaged to a time resolution of one minute. Lengths of the lines reflect average total wave intensities in magnetic components on a logarithmic scale between 10^{-7} and 10^{-4} nT^{2}Hz^{-1}. (a) Results for a frequency interval 620–640 Hz; (b) Results for a higher frequency interval 780–820 Hz.

inclined toward the equator at lower latitudes below 62° (approximately snapshot 12 on Figure 1) and toward the pole at higher latitudes.

3. Interpretation and Reverse Ray Tracing

[16] The analysis shows a divergent propagation pattern of the downgoing hiss emission and band-limited poleward and upward propagating waves at higher latitudes. These upgoing waves can be interpreted as a reflected poleward propagating portion of the originally downgoing hiss. This reflection process should take place at altitudes below the satellite orbit. There are several reasons supporting this hypothesis. First, the wave vector directions of upgoing waves are well consistent with reflection of the poleward propagating part of downgoing hiss. Second, the wave distribution function analysis of *Santolík and Parrot* [2000] showed peaks of both upgoing and downgoing waves at the same time and frequency. The directions of these peaks are consistent with nearly specular reflection. The spectra of ELF hiss emissions indicate a probable reflection mechanism. In the downgoing part, a sharp lower cutoff just below the local f_{H^+} suggests the reflection at the multiion cutoff frequency (f_{cL}) [*Gurnett and Burns*, 1968].

[17] We believe that this hypothesis also explains the band limitation of poleward propagating upgoing hiss. Its lower-frequency limit ($\approx$500 Hz) must lie close to the local f_{cL}, corresponding to the local reflection. The upper-frequency limit then corresponds to f_{cL} at the lowest possible altitude of reflection below the spacecraft. Supposing a very

low hydrogen fraction at these altitudes, we have f_{cL} very close to the local f_{H^+}. For our case, wave intensity starts to decrease at about 700 Hz, which corresponds to a reflection height of 580 km ($\approx$620 km below the spacecraft position); it reaches one half of the original amplitude around 750 Hz (reflection at about 430 km); and finally, it decreases down to the background level at 780 Hz (reflection height of 350 km, i.e., approximately 850 km below the spacecraft). Under this hypothesis, the reflection coefficient would strongly decrease with altitude from 580 km to 350 km. Below 350 km, the reflection would be impossible, probably as a consequence of a higher collision rate and/or a low hydrogen fraction.

[18] We thus consider the upward propagating waves at higher latitudes as a secondary phenomenon connected to the originally downward propagating emission. To examine its propagation we first calculate local parameters of a typical wave from the cold plasma theory. We use experimentally obtained plasma parameters: plasma density measured by the Langmuir probe and the magnetic field data measured by the F2 fluxgate magnetometer [*FREJA magnetic field experiment team*, 1994]. The ion composition is obtained from the position of the sharp lower cutoff of downgoing ELF hiss,

$$f_{cL} = f_{H^+} \frac{1 + P_O (R_{OH} - 1)}{R_{OH}}, \qquad (1)$$

where P_O is the relative fraction of oxygen ions, and $R_{OH} \approx$ 16 is the ratio of masses of oxygen to hydrogen ions. With
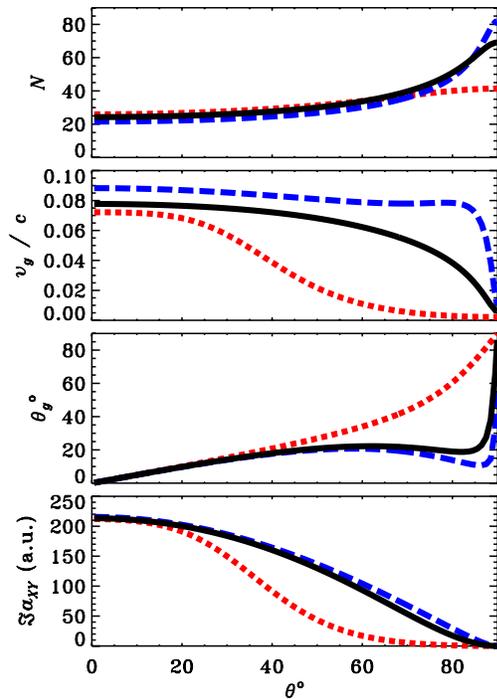
Figure 3. Theoretical wave properties calculated for the cold plasma model which has been inferred from observations. The data are plotted versus the θ angle between the wave vector and the static magnetic field. From the top: wave refractive index N, group velocity (v_g) normalized to the speed of light (c), angle deviation (θ_g) of the group velocity from the static magnetic field, imaginary part of the cross-spectrum between the perpendicular B_x and B_y components of magnetic fluctuations ($\Im a_{XY}$). The frequency of 1.17 f_{H^+} = 624 Hz is represented by the solid line, the results at two other frequencies are given by the dotted line (1.01 f_{H^+} = 540 Hz), and by the dashed line (1.50 f_{H^+} = 800 Hz).

the measured hydrogen cyclotron frequency (f_{H+} = 534 Hz) and multiion cutoff frequency (f_{cL} = 521 Hz) we obtain a plasma model with 3% of hydrogen ions. The rest of the ion component of the plasma is supposed to be constituted by the singly charged oxygen. The same result is obtained from the value of the lower hybrid frequency identified with the lower cutoff of electrostatic waves at 3.7 kHz (not shown) and from the measured electron plasma frequency (f_p = 620 kHz).

[19] With this model of the medium, we use the cold plasma theory [*Gurnett and Bhatacharjee*, 2005] to calculate wave properties. The results are qualitatively similar for the entire hiss emission, and in Figure 3 we show several wave parameters plotted versus the angle deviation (θ) between the wave vector and the static magnetic field. Results are given at three different frequencies between f_{H^+} and the lower hybrid frequency f_{lh} where a single cold-plasma wave mode can propagate. At these frequencies, there is no oblique resonance, and the wave refractive index (N) has finite values for all θ. However, at frequencies above f_{H^+}, N significantly grows with θ, and the rapid increase stops only for nearly perpendicular propagation.

This behavior has consequences for the direction of the group velocity: its angle deviation from $\mathbf{B_0}$ is below about $20°$ in the majority of the θ interval. Only for θ very close to $90°$, the group velocity abruptly turns to the perpendicular direction. The frequency variation of the refractive index implies that the group velocity modulus is higher at lower θ and higher frequencies. The bottom panel shows the imaginary part of the cross-spectrum between the two magnetic components perpendicular to the static magnetic field. Positive values correspond to the right-handed polarization consistent with the observations.

[20] It is thus clear that the group velocity is less deviated from the static magnetic field than the wave vector but from Figure 2 we can still estimate the point where wave propagation turns from the equatorward to the poleward direction: at the altitude of observation, it is located at a magnetic latitude slightly above $60°$ (McIlwain's L $\approx$ 4.6) and at a magnetic local time between 6 and 7 hours. This divergent propagation pattern might correspond to a rather localized source of the hiss emission, and it is important to know whether the "turning point" lies inside or outside the plasmasphere. The local plasma density measurements do not show any distinct density gradient after the beginning of the data record. The only change of plasma parameters is observed indirectly using the wave measurements up to 16 kHz. The lower cutoff of electrostatic VLF hiss decreases just in the beginning of the data record, before 1548 UT (not shown). Interpreting this cutoff as the local lower hybrid frequency, and assuming a nearly constant plasma density, we attribute this decrease to changes in the ion composition. The satellite entered the light ion trough where oxygen ions are prevailing. All these observations lead us to the conclusion that the entire data record, including the "turning point," lies outside of the plasmasphere and, probably, the same holds true also for the source region.

[21] These intuitive estimates are confirmed by results of backward ray tracing. We use a modified version of the three-dimensional procedure of *Cairó and Lefeuvre* [1986]. We follow the wave rays backward from the point of observation. The procedure is initialized by a reversed wave normal direction $\mathbf{k}$ found experimentally at low altitudes. For a given dispersion relation

$$\omega = \omega(\mathbf{x}, \mathbf{k}, \mathbf{t}), \tag{2}$$

where $\omega = 2\pi f$, we have, under the approximation of the geometric optics,

$$\frac{d\mathbf{x}}{dt} = \frac{\partial \omega}{\partial \mathbf{k}} \tag{3}$$

$$\frac{d\mathbf{k}}{dt} = -\frac{\partial \omega}{\partial \mathbf{x}} \tag{4}$$

[22] This set of differential equations describing the ray trajectories is numerically integrated using the Runge-Kutta fourth-order method with one midpoint and adaptive integration step to obtain evolution of the position of the ray $\mathbf{x}$ and the corresponding wave vector $\mathbf{k}$ as a function of the group time t. This procedure has been recently improved

(a)

(b)
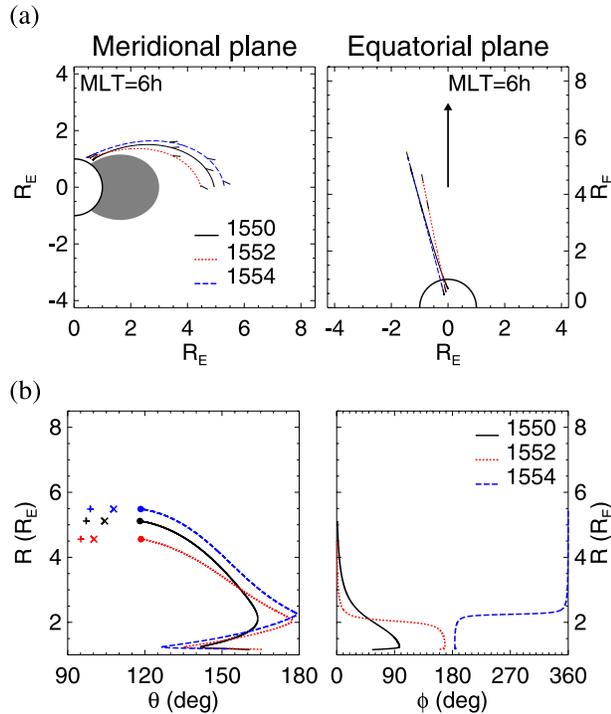
Figure 4. Results of the backward ray tracing for a diffusive equilibrium plasma model with a temperature of 1000 K. Three sets of boundary conditions are used according to the observed wave vector directions along the spacecraft orbit for three time intervals, centered respectively at 1550 (solid line), 1552 (dotted line), and 1554 (dashed line). (a) Ray traces plotted in two orthogonal projections, respectively, to the plane of the geomagnetic equator, and to the plane of the magnetic meridian at MLT = 6 h. The arrows plotted along the traces show the wave vector directions at times separated by 0.5 s of the ray propagation (group) time. (b) Wave vector direction described by angle θ from the static magnetic field and by the azimuth angle ϕ from the magnetic meridian plane. θ at the geomagnetic equator (filled circles) is compared to the local resonance angle (plus signs) and to the local Gendrin angle (crosses).

from the version of *Cairó and Lefeuvre* [1986], as well as the wave mode control and convergence criteria. In every integration step we verify the Wentzel-Kramers-Brillouin (WKB) approximation of geometric optics. The ray is not followed beyond the limit where this fundamental approximation becomes invalid. We use a dipolar approximation of the magnetic field and a diffusive equilibrium model for ion and electron densities. This plasma density model is calibrated by the observed plasma parameters at an altitude of 1000 km, using the above described model of a two component plasma with hydrogen and oxygen ions.

[23] To extrapolate this plasma model to higher altitudes according to the diffusive equilibrium law, we also need an estimate of the plasma temperature. However, we have no experimental information about the plasma temperature at the spacecraft altitude. As it is a crucial parameter of the model, we have run the ray tracing procedure with density models for different temperatures.

[24] The boundary conditions for the ray tracing equations were defined using the wave vector measurement at the spacecraft orbit in the same frequency interval as the one used in Figure 2b: a 40-Hz interval centered at 800 Hz. We use a two-minute average of the data centered around three separate points along the orbit reached at 1550, 1552, and 1554 (McIlwain's L of 3.65, 5.14, and 7.61, respectively). From each of these points a ray was integrated until it encountered the geomagnetic equator.

[25] In Figures 4 and 5 we present the results for models with temperatures of 1000 K and 5000 K, respectively. The 1000-K model gives a higher but still realistic equatorial plasma density of about 80 cm^{-3} at a radial distance of 4 R$_E$, whereas the 5000-K model gives these densities close to 500 cm^{-3} which would be rather typical for an extended plasmasphere. Three ray traces are plotted in two orthogonal projections. As expected, the low-altitude propagation pattern is consistent with rays confined initially to a relatively narrow beam. At larger radial distances from the Earth the ray trajectories depend on the temperature controlling the diffusive equilibrium model. For the 5000-K model the rays cross the equator at L between 5.8 and 6.5. For the 1000-K model, the rays stay slightly closer to the Earth; they cross the equator at L between 4.6 and 5.5. Although the initial wave normals at low altitudes have considerable azimuthal ϕ angles (45°, 160°, and 185°), along the raypath these values rapidly decrease and near the equator they approach 0°. This means that the reverse wave vector is directed outwards from the Earth in the plane of the local magnetic meridian. At high altitudes the waves thus propagate close to the meridional plane.

[26] Important results can be obtained by analyzing the evolution of the θ angle (declination of the wave vector

(a)

(b)
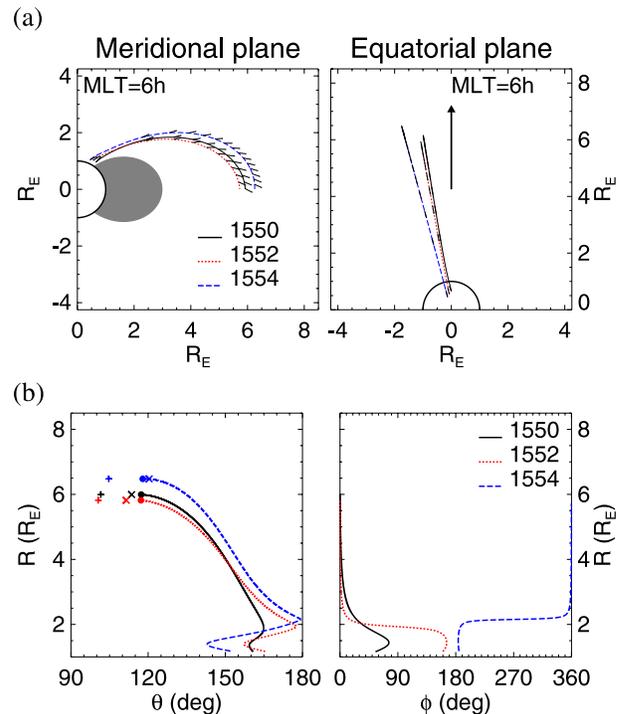
Figure 5. The same as in Figure 4 but for a plasma model with a temperature of 5000 K.

(a)

(b)
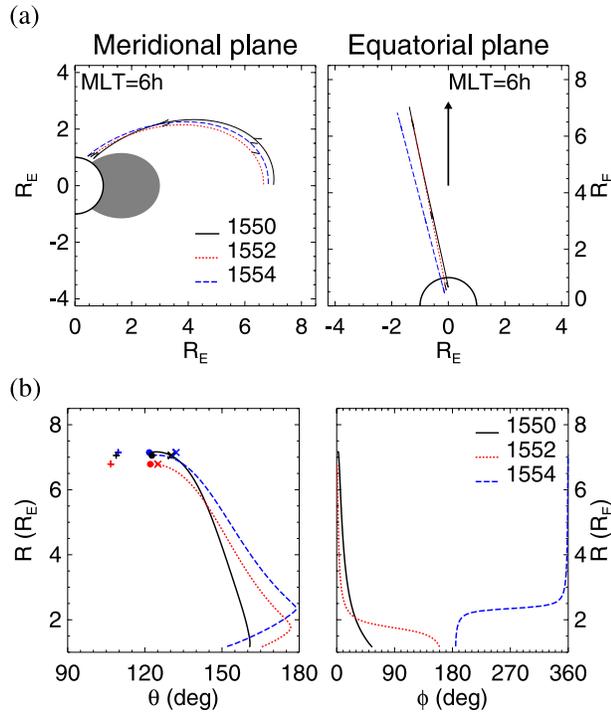
Figure 6. The same as in Figure 4 but for a plasma model with a density decreasing as R^{-4} and a simplified ray tracing procedure.

from the static magnetic field) along the raypath. For all rays, the wave vectors become more anti-field-aligned at radial distances between 0.9 and 1.3 R_E where the rays reach magnetic latitudes around 42–47°. Then, θ values start to decrease again, and at the equator the wave vectors are inclined by about 120° from the ambient magnetic field. This is close to the local Gendrin angle and thus the ray directions, being parallel to group velocity, remain nearly field aligned in this region. For the 1000-K model the ray direction is within 13° from antiparallel to the static magnetic field at the equator. For the 5000-K model it is even closer, within 4° from the field line. Recall that the plasma density at high altitudes is higher and, consequently, the group speed is lower for the 5000-K model than for the 1000-K model. This is shown by different spacings of the arrows plotted along the traces in Figures 4 and 5.

[27] Very similar results, shown in Figure 6, have been obtained using a different ray-tracing procedure described by *Shklyar and Jiříček* [2000]. This method uses an approximation of the cold-plasma dispersion relation which is valid in the frequency range between the ion and electron cyclotron frequencies and in the high density limit. The technique implements a gyrotropic distribution of plasma density where the density is proportional to a general power of the cyclotron frequency. For a given latitude, the plasma density model can thus be defined as decreasing with a predefined power of the radial distance while the density at an altitude of 1000 km is given by the measurement. Figure 6 shows the results for the density proportional to R^{-4}. With this density model, the rays cross the magnetic equatorial plane at radial distances from 6.8 to 7.1 R_E. The R^{-4} model gives a realistic density of 16 cm^{-3} at R = 4 R_E.

This model also well corresponds to the plasma densities which were previously observed outside the plasmasphere [*Angerami and Carpenter*, 1966]. Evolution of the wave normal direction for the R^{-4} model (Figure 6b) also shows the initial anti-field-aligned propagation at radial distances around 2 R_E and propagation close to the local Gendrin angle at the equator, with wave vectors directed outwards from the Earth. Recall, that these results are obtained from reverse ray tracing simulations. The way in which the wave would propagate from its source region would thus be exactly opposite to the obtained results: with wave vectors directed toward the Earth in the plane of the local magnetic meridian.

[28] The results at a lower frequency of 630 Hz, corresponding to Figure 2a, are very similar. The reverse rays reach similar region in the equatorial plane, with nearly the same evolution of the θ angle along the raypath. However, differences are obtained for the group time calculated form the spacecraft orbit to the equatorial plane. For example, the 1000-K model gives the group time at 630 Hz by $\approx$16% (160 ms) longer than at 800 Hz.

[29] Hypothetically, the source region may be located anywhere along the raypaths of observed low-altitude ELF hiss. However, special conditions occur in the equatorial region. A propagating wave packet of a given frequency can be, for example, amplified by a cyclotron resonance with energetic electrons. The energy of resonant electrons mainly depends on the local plasma density, the wave-normal angle θ, and on the strength of the static magnetic field. In the equatorial region, a wave packet propagating approximately along the field line (which, as we have shown, is our case) encounters a minimum of the static magnetic field. Here, the wave packet can be in resonance with electrons of approximately the same energy for a much longer time than anywhere else along its path, supposing that the density variations along the field line are negligible. Thus a possible candidate of the source region is the equatorial plane outside of the plasmapause, at L between 5 and 7. This is likely the same location as in the case of the source region of whistler mode chorus, as it has been, for lower L, recently shown using the Poynting flux data of the Polar spacecraft [*LeDocq et al.*, 1998], and for the lower-band chorus below $0.5f_{ce}$, also using similar measurements of the Cluster spacecraft [*Parrot et al.*, 2003; *Santolík et al.*, 2004, 2005].

4. Comparison With Whistler Mode Chorus

[30] The possible colocation of the source regions of the whistler mode chorus and low-altitude ELF hiss opens a possibility for a hypothesis that the observed ELF hiss is a low altitude manifestation of chorus. Our reverse ray tracing analysis shows that hiss is composed of waves which could come from a sufficiently wide region of the order of 1 R_E in the equatorial plane. In such a case we can suppose that many individual chorus wave packets would be dispersed and superposed, forming a homogeneous hiss-like emission. Indeed, *Chum and Santolík* [2005] have shown that a point source of chorus located close to the equator at different radial distances can emit nonducted divergent rays, some of which penetrate down to the topside ionosphere or, possibly,
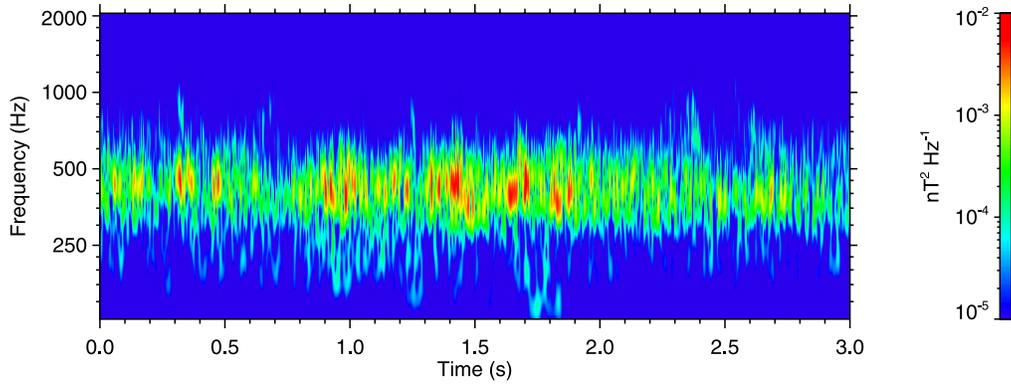
Figure 7. Wavelet power as a function of time and frequency calculated from a waveform of the magnetic B_y component recorded during a single 3-s snapshot no. 24 (see Figure 1), starting at 1553:05.345 UT.

to the ground. The chorus wave packets from these individual sources can be then superposed at the given latitude.

[31] Nevertheless, a residual frequency-time structure resembling original discrete wave packets of chorus might still be conserved in the low-altitude emission. Figure 7 shows results of detailed analysis of a single 3-s snapshot of data from the spectrogram in Figure 1. To increase the time-frequency resolution we have used an analysis technique based on Morlet wavelets [*Lagoutte et al.*, 1992]. The analysis has included 4 octaves from 128 to 2048 Hz, with increasing time resolution at higher frequencies. The results are presented in the form of power spectrograms of the same component of the fluctuating magnetic field as in Figure 1. We can see that at these very short timescales, the ELF hiss surprisingly reveals fine time-frequency structure. Very similar structures have been also found in other snapshots during the analyzed time interval. Other cases of Freja observations of ELF hiss also show similar structures, when wave bursts often arrive in a larger-frequency band nearly at the same time. Taking into account the group delay which would affect wave packets propagating from the equatorial region, the observed structures might correspond to realistic chorus with a frequency drift of a few kHz/s for individual wave packets.

[32] We have analyzed several cases of ELF hiss recorded by the recently launched low-altitude spacecraft DEMETER and we have obtained similar results. An example is shown in Figure 8. In its ELF frequency range and during the burst-mode, the IMSC instrument [*Parrot et al.*, 2006] onboard DEMETER measures the waveforms of three magnetic components with a sampling rate of 2.5 kHz. Figure 8 shows the results of the wavelet analysis using 3 seconds s of the B_x magnetic field component (perpendicular to the static magnetic field, in the plane of the local magnetic meridian). We again use the Morlet wavelets. The data were recorded when the low-altitude ELF hiss was observed in the morning sector, at a MLT of 1023. The magnetic latitude was 52.5°, which, for an altitude of 709 km, corresponds to a McIlwain's L parameter of 2.95. This means that these observations are at a lower latitude than the previously discussed case recorded by the Freja spacecraft. However, fine time-frequency structures resembling the chorus elements are also detected in this case. The spacecraft is located in the light ion trough outside of the plasmasphere during that time period, based in the onboard ion composition measurement. The plasmaspere is most probably contracted after a disturbed period with Kp index reaching 7^+ 24 hours before the event and slowly decreasing down to
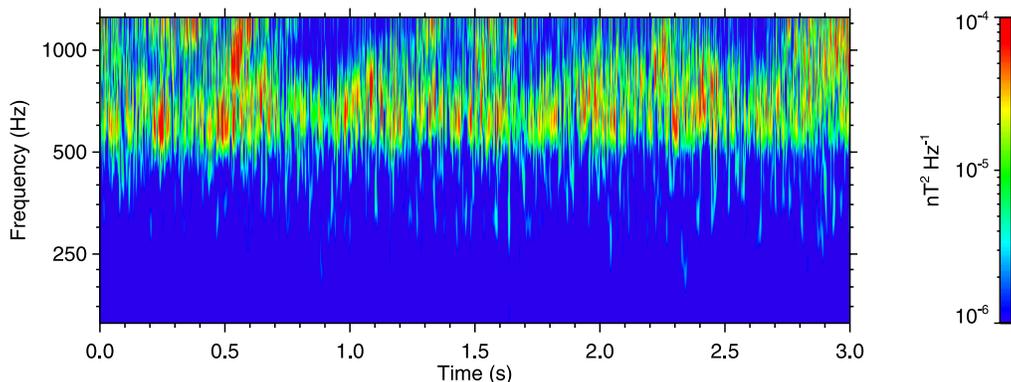
Figure 8. Detail of observations of the DEMETER spacecraft on 13 June 2005. Three seconds of measurements of the B_x magnetic field component starting at 1911:54.136 UT have been processed by the same method as in Figure 7.
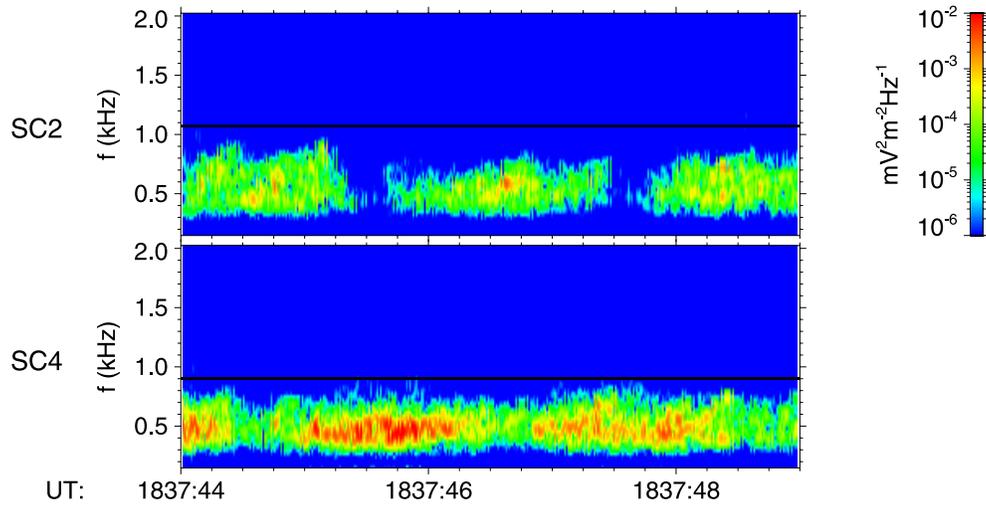
Figure 9. Cluster observations on 14 October 2001. The electric field fluctuations measured by the WBD instrument are plotted as time-frequency spectrograms for two spacecraft, Cluster 2 and Cluster 4 at L = 7.35 and L = 7.77, respectively. The 2-s modulation seen on both spectrograms is owing to the spin of the spacecraft. Black horizontal lines correspond to 0.5 f_{ce0} obtained using equation 5.

Kp = 3$^+$ during the measurement, giving the average plasmapause at L of 2.4 according to the model of *Carpenter and Anderson* [1992].

[33] The question arises as to whether these structured emissions really can correspond to whistler mode chorus in the observed frequency range. To demonstrate this possibility we would have to record chorus in the same frequency interval at higher altitudes, coinciding with a place close to the backward raypaths of the ELF hiss. Figures 9, 10, and 11 present such demonstration using measurements of the Cluster spacecraft.

[34] Figure 9 shows measurements of the WBD instruments [*Gurnett et al.*, 2001] on board of two Cluster spacecraft. Cluster 2 and Cluster 4 are, respectively, located at a radial distance of 4.84 R_E and 4.77 R_E, at a magnetic latitude of $-35.7°$ and $-38.4°$, and at a MLT of 0953 and 0958. The corresponding McIlwain's parameters are L =

7.35 and L = 7.77. Figure 10 shows another selected data interval recorded by the same spacecraft but at a slightly lower L-shell. During this second time interval, Cluster 2 and Cluster 4 are, respectively, at a radial distance of 4.65 R_E and 4.57 R_E, at a magnetic latitude of $-28.8°$ and $-31.3°$, at a MLT of 0947 and 0952, and at L = 6.06 and L = 6.26.

[35] The wave emission observed by both Cluster spacecraft contains discrete time-frequency structures of whistler mode chorus. The waves are always related to the projection of the locally measured electron cyclotron frequency along the dipolar field lines to the equatorial plane,

$$f_{ce0} = f_{ce} \frac{\cos^6 \lambda_m}{\sqrt{1 + 3 \sin^2 \lambda_m}}, \quad (5)$$
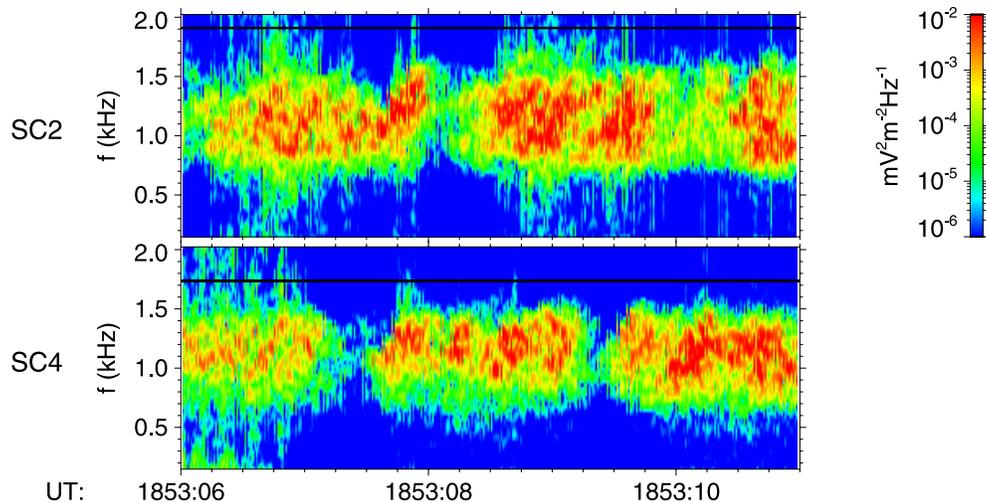
Figure 10. The same as in Figure 9 but for another time interval on 14 October 2001. Cluster 2 and Cluster 4 are at a lower L shell of 6.06 and 6.26, respectively.
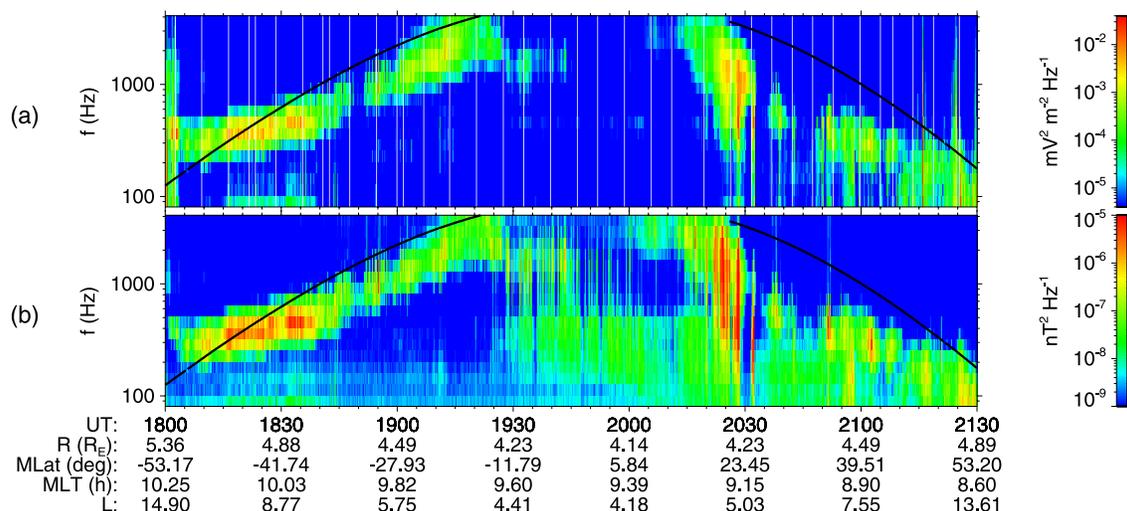
Figure 11. Cluster-4 observations on 14 October 2001. (a) Time-frequency power spectrogram of electric field fluctuations. (b) Time-frequency power spectrogram of magnetic field fluctuations measured by the STAFF-SA instrument. Black line is one half of the equatorial electron cyclotron frequency obtained using equation (5).

where λ_m is the magnetic latitude of the spacecraft. Note, comparing the two Cluster spacecraft in Figure 9, that the frequencies of chorus are slightly different, and that they correspond to differences of 0.5 f_{ce0} at the given spacecraft. As the spacecraft move to lower λ_m and lower L shells (see Figure 10), the frequencies of intense chorus become substantially higher, according to the increase of 0.5 f_{ce0} from equation (5). Note also, that the two spacecraft do not simultaneously observe the same fine time-frequency structure of chorus wave packets. This is consistent with conclusions of *Santolík and Gurnett* [2003] and *Santolík et al.* [2004] on the correlation length of chorus wave packets, taking into account that the separation of Cluster 2 and Cluster 4 is approximately 1600 km (≈1400 km if measured in the plane perpendicular to the field line).

[36] Simultaneous measurements of the STAFF-SA instrument [*Cornilleau-Wehrlin et al.*, 2003] onboard the same spacecraft demonstrate that these waves are electromagnetic and right-hand polarized, propagating from the equator toward higher latitudes, and, consequently, to lower altitudes. Figure 11 shows STAFF-SA data for Cluster 4 (data from Cluster 2 and the other two Cluster spacecraft give similar results). Both the spectrogram of the electric field fluctuations (Figure 11a) and magnetic field fluctuations (Figure 11b) demonstrate that the wave frequencies of chorus are most of the time below 0.5 f_{ce0} from equation (5). From simultaneous measurement of the magnetic and electric fluctuations we can calculate the parallel component of the Poynting flux and the electromagnetic planarity (not shown) using the method of *Santolík et al.* [2003b]. These results demonstrate that the waves propagate from the source region located within ≈5° of magnetic latitude from the equatorial plane.

[37] The latitudes where chorus is observed, as shown in Figure 11, are close to those resulting from the ray tracing simulations for a given radial distance. The observed chorus frequencies between 200 Hz and 2 kHz are also consistent with the above described low altitude observations by the

Freja and DEMETER spacecraft. Furthermore, the wave vector direction of these waves measured onboard Cluster are inclined by 30–50° from the static magnetic field (not shown). This is consistent with the results of the reverse ray tracing simulations for the same radial distance, as presented in Figures 4–6. Note that the wave vector direction in this simulation is antiparallel to the observed directly propagating wave, i.e., its inclination from the static magnetic field is ≈130–150°.

5. Discussion and Conclusions

[38] The downward divergent propagation pattern of low-altitude ELF hiss does not seem to be a special feature of the particular cases discussed in this paper but rather is a general property of this type of emission. Similar results have been reported from other measurements of the Freja spacecraft [spectral type A of *Santolík and Parrot*, 1999] and also from the data set of the Aureol-3 spacecraft [*Lefeuvre et al.*, 1992]. Since the propagation analysis requires multicomponent measurements of the wave electric and magnetic fields it could not be previously reported from other spacecraft without appropriate experimental devices. These observations are, however, consistent with a number of previously reported measurements [e.g., *Gurnett and O'Brien*, 1964; *Taylor and Gurnett*, 1968; *Mosier*, 1971; *Barrington et al.*, 1971].

[39] Upgoing waves are also observed in the presented case and in other cases of low-altitude ELF hiss. We consider these upward propagating emissions to be secondary phenomena, originating from downward propagating hiss. The observations are consistent with reflection of downward hiss at the f_{cL} cutoff (equation (1)) at lower altitudes below the spacecraft. The reflection can occur both poleward [*Santolík and Parrot*, 2000] and equatorward (spectral type F of *Santolík and Parrot* [1999]) from the subauroral latitudes where the divergent downgoing ELF hiss is observed.

[40] The latter type of secondary upward propagating waves was most often observed at magnetic latitudes below 55° [e.g., *Mosier*, 1971; *Lefeuvre et al.*, 1992; *Santolík and Parrot*, 1999]. Reflected hiss then can further propagate into the plasmasphere. These waves can, hypothetically, be considered as a possible candidate for the embryonic source of plasmaspheric hiss, which is still controversial [see *Storey et al.*, 1991; *Draganov et al.*, 1992; *Hayakawa and Sazhin*, 1992; *Santolík et al.*, 2001, and references therein]. *Green et al.* [2005] has recently presented evidence on lightning-induced whistlers as the embryonic source of plasmaspheric hiss. Equatorward reflected ELF hiss which, as we show, is most probably related to chorus emissions might represent another simultaneously acting embryonic source, subsequently amplified by a mechanism proposed by *Solomon et al.* [1988] and *Cornilleau-Wehrlin et al.* [1993]. The dependence of plasmaspheric hiss on the substorm activity, reported by *Meredith et al.* [2004], might be in favor of the chorus-related embryonic source.

[41] Other wave emissions originating from the downward propagating ELF hiss are down-going field aligned waves below the local f_{H+} which also demonstrate similar occurrence pattern [*Santolík and Parrot*, 1998]. These waves (spectral type B of *Santolík and Parrot* [1999]) most probably penetrate to these frequencies at higher altitudes above the spacecraft by tunnelling of ELF hiss below the multiion cross-over frequency [*Santolík and Parrot*, 1998].

[42] All the three above mentioned types of secondary emissions should have the same original source, coinciding with the source of primary emissions of downward propagating ELF hiss. The predominant high-latitude occurrence of hiss was previously found by many low-altitude measurements [e.g., *Taylor and Gurnett*, 1968; *Barrington et al.*, 1971; *Parrot*, 1990; *Lefeuvre et al.*, 1992], and the cases we analyzed represent an attempt to explain the origin of this large class of wave phenomena. Using the initial wave vectors measured at low altitudes, our reverse ray tracing study indicates that the source might be located close to the geomagnetic equator at radial distances of $5-7$ R$_E$.

[43] This location coincides with the source region of whistler mode chorus [*LeDocq et al.*, 1998; *Lauben et al.*, 2002; *Parrot et al.*, 2003; *Santolík et al.*, 2004, 2005]. Possible connection of low-altitude ELF hiss with chorus is supported by the fact that ELF hiss is predominantly observed on the dayside and has thus a very similar local-time occurrence as chorus. More importantly, discrete time-frequency structures, resembling chorus wave packets have been detected in ELF hiss by a detailed analysis of measured waveforms. A term "structured hiss" would thus be more appropriate for the description of these emissions.

[44] Indeed, in situ measurements of chorus show that its frequencies and wave vector directions along the simulated reverse raypaths of ELF hiss are consistent with the hypothesis that ELF hiss is a low altitude manifestation of chorus. Since the individual chorus wave packets are necessarily dispersed and mixed together during their unducted propagation to lower altitudes [*Parrot et al.*, 2004b], the underlying discrete structure of ELF hiss is not easily detectable. Its appearance on the time-frequency spectrograms is thus often more diffuse and hiss-like compared to cases of ducted chorus observed on the ground [e.g., *Smith et al.*, 2004], although cases similar to the "structured hiss" can be found also on the ground [see *Horne et al.*, 2005, Figure 2]. The origin and source region of "structured hiss" and ducted chorus are most probably the same.

[45] Another reason for apparent absence of discrete structures in the low-altitude ELF hiss is that the original chorus-like emissions often do not contain any discrete structures already in their source region. These waves with structureless spectrograms which propagate from chorus source region can be quite often found in the data of the WBD and STAFF-SA instruments onboard the Cluster spacecraft. Similar behavior of the chorus source is also predicted by the nonlinear backward wave oscillator theory of chorus generation [*Trakhtengerts*, 1999].

[46] The observed low-altitude structured hiss also has another property which is much more similar to chorus than to plasmaspheric hiss. The analysis of coherence of the three measured magnetic components [*Santolík and Parrot*, 2000] shows that the downward propagating waves are very coherent, with a degree of polarization close to 1. Similar analysis performed on board the GEOS spacecraft by *Cornilleau-Wehrlin et al.* [1978] and *Lefeuvre and Parrot* [1979] clearly indicates that such a high coherency is typical for chorus and that the plasmaspheric hiss shows significantly lower values.

[47] The backward ray tracing simulation leads us to somewhat special requirements for wave normal directions of the original chorus waves in their source region. The wave vectors have to be substantially oblique with respect to the field line and directed toward the Earth. A direct ray tracing study of *Chum and Santolík* [2005] shows that there is no other possibility for chorus waves to penetrate to low altitudes. The angle between the wave vector and the static magnetic field in the chorus source region has to be approximately 60°. This is close to the local Gendrin angle for which the group velocity of the waves is again close to field-aligned. However, lower-band chorus below 0.5 f_{ce0} is often observed with an average wave vector direction along the field lines in its source [e.g, *Hayakawa et al.*, 1984; *Santolík et al.*, 2003a] although highly inclined wave vectors were also observed directly inside the generation region [*Santolík et al.*, 2003a]. The penetration of chorus/ELF hiss to low altitudes can then be explained by these latter observations or by the possibility that the spectrum of wave normal directions contains highly inclined wave vectors although its average appears to be along the field line. The Earthward direction most probably does not have any special importance for the source mechanism. If highly oblique wave vectors are generated in all azimuthal directions around the field line, only those which are inclined toward the Earth can penetrate to low altitudes.

[48] However, theoretical approaches to the generation of chorus mostly suppose quasi-parallel wave vector directions, and large angles between the wave vectors of unstable waves and the local magnetic field might require a modification of existing theories on chorus source mechanism. Generation of chorus with wave vectors close to the Gendrin angle has previously been deduced by *Lauben et al.* [2002] from a ray tracing study. *Storey et al.* [1991] also found that hiss may be generated at highly oblique wave vectors and suggested that this instability may probably be nonlinear. The propagation near the Gendrin angle could be

an important feature of this mechanism. It is well possible, though, that only a minor part of all the observable chorus emissions (those which can penetrate to low altitudes in the unducted mode) might be generated by this mechanism. The majority of chorus might still be generated with quasi-parallel wave vectors but those waves would only be observable at higher altitudes or in the density ducts. More measurements of wave vector directions, ray-tracing and/or statistical studies are needed to resolve this problem.

[49] The main conclusion of this study is that chorus or chorus-like waves, generated with highly oblique wave vectors in a source region located close to the geomagnetic equator outside the plasmasphere at radial distances above 5 R_E, are very likely source emissions of a large class of low-altitude wave phenomena, including (1) downward propagating ELF hiss occurring at subauroral latitudes; (2) downward propagating right hand polarized ELF hiss emissions below the local proton cyclotron frequency; (3) upward propagating ELF hiss at higher latitudes in the auroral region and polar cap; (4) upward propagating ELF hiss at middle and low latitudes, representing one of the potential embryonic sources of plasmaspheric hiss. We have found several independent arguments to support the hypothesis that all these frequently observed day side ELF hiss events can originate from whistler mode chorus: (1) both chorus and low-altitude ELF hiss predominantly occur on the local morningside and dayside; (2) both chorus and low-altitude ELF hiss show high coherency of the measured magnetic field components; (3) discrete time-frequency structures have been detected in low-altitude ELF hiss; (4) a reverse ray tracing study, involving the in situ measured wave vector directions of ELF hiss, shows that frequencies and wave vector directions along the reverse raypaths are consistent with chorus observations. Further studies of conjugated low- and high-altitude observations are underway and the results will be reported when they become available.

References

Aarons, J., G. Gustafsson, and A. Egeland (1960), Correlation of audio-frequency electromagnetic radiation with auroral zone micropulsations, *Nature*, *185*, 148–151.

Angerami, J. J., and D. L. Carpenter (1966), Whistler studies of the plasmapause in the magnetosphere: 2. Electron density and total tube content near the knee in magnetospheric ionization, *J. Geophys. Res.*, *71*, 711–725.

Barrington, R., T. Hartz, and R. Harvey (1971), Diurnal distribution of ELF, VLF and LF noise at high latitudes as observed by Alouette 2, *J. Geophys. Res.*, *76*, 5278–5291.

Burtis, W. J., and R. A. Helliwell (1976), Magnetospheric chorus: Occurrence patterns and normalized frequency, *Planet. Space Sci.*, *24*, 1007–1024.

Cairó, L., and F. Lefeuvre (1986), Localization of sources of ELF/VLF hiss observed in the magnetosphere: Three-dimensional ray tracing, *J. Geophys. Res.*, *91*, 4352–4364.

Carpenter, D. L., and R. R. Anderson (1992), An ISEE/whistler model of equatorial electron density in the magnetosphere, *J. Geophys. Res.*, *97*, 1097–1108.

Chum, J., and O. Santolík (2005), Propagation of whistler mode chorus to low altitudes: Divergent ray trajectories and ground accessibility, *Ann. Geophys.*, *23*, 3727–3738.

Cornilleau-Wehrlin, N., R. Gendrin, F. Lefeuvre, M. Parrot, R. Grard, D. Jones, A. Bahnsen, E. Ungstrup, and W. Gibbons (1978), VLF electromagnetic waves observed onboard GEOS-1, *Space Sci. Rev.*, *22*, 371–382.

Cornilleau-Wehrlin, N., J. Solomon, A. Korth, and G. Kremser (1993), Generation mechanism of plasmaspheric ELF hiss: A statistical study from GEOS 1 data, *J. Geophys. Res.*, *98*, 21,471–21,479.

Cornilleau-Wehrlin, N., et al. (2003), First results obtained by the Cluster STAFF experiment, *Ann. Geophys.*, *21*, 437–456.

Draganov, A. B., U. S. Inan, V. S. Sonwalkar, and T. F. Bell (1992), Magnetospherically reflected whistlers as a source of plasmaspheric hiss, *Geophys. Res. Lett.*, *19*, 233–236.

FREJA magnetic field experiment team (1994), Magnetic field experiment on the Freja satellite, *Space Sci. Rev.*, *70*, 465–482.

Green, J. L., S. Boardsen, L. Garcia, W. W. L. Taylor, S. F. Fung, and B. W. Reinisch (2005), On the origin of whistler mode radiation in the plasmasphere, *J. Geophys. Res.*, *110*, A03201, doi:10.1029/2004JA010495.

Gurnett, D. A., and A. Bhatacharjee (2005), *Introduction to Plasma Physics With Space and Laboratory Applications*, Cambridge Univ. Press, New York.

Gurnett, D. A., and T. B. Burns (1968), The low-frequency cutoff of ELF emissions, *J. Geophys. Res.*, *73*, 7437–7445.

Gurnett, D. A., and B. J. O'Brien (1964), High-latitude geophysical studies with satellite Injun 3: 5. Very-low-frequency electromagnetic radiation, *J. Geophys. Res.*, *69*, 65–89.

Gurnett, D. A., et al. (2001), First results from the Cluster wideband plasma wave investigation, *Ann. Geophys.*, *19*, 1259–1272.

Hayakawa, M., and S. S. Sazhin (1992), Mid-latitude and plasmaspheric hiss: A review, *Planet. Space Sci.*, *40*, 1325–1338.

Hayakawa, M., Y. Yamanaka, M. Parrot, and F. Lefeuvre (1984), The wave normals of magnetospheric chorus emissions observed on board Geos 2, *J. Geophys. Res.*, *89*, 2811–2821.

Hayakawa, M., F. Lefeuvre, and J. Rauch (1985), The direction finding aboard AUREOL-3 of ELF waves at frequency above and below the proton gyrofrequency, in *CNES-Results of the ARCAD-3 Project and of the Recent Programmes in Magnetospheric and Ionospheric Physics*, p. 499, Cepadues, Toulouse, France.

Helliwell, R. A. (1967), A theory of discrete emissions from the magnetosphere, *J. Geophys. Res.*, *72*, 4773–4790.

Holback, B., S.-E. Jansson, L. Ahlen, G. Lundgren, L. Lyngdal, S. Powell, and A. Meyer (1994), The Freja wave and plasma density experiment, *Space Sci. Rev.*, *70*, 577–592.

Horne, R. B., S. A. Glauert, and R. M. Thorne (2003), Resonant diffusion of radiation belt electrons by whistler mode chorus, *Geophys. Res. Lett.*, *30*(9), 1493, doi:10.1029/2003GL016963.

Horne, R. B., et al. (2005), Wave acceleration of electrons in the Van Allen radiation belts, *Nature*, *437*, 227–230, doi:10.1038/nature03939.

Koons, H. C., and J. L. Roeder (1990), A survey of equatorial magnetospheric wave activity between 5 and 8 R_E, *Planet. Space. Sci.*, *38*(10), 1335–1341.

Laaspere, T., M. G. Morgan, and W. C. Johnson (1964), Chorus, hiss, and other audio-frequency emissions at stations of the Whistlers-East network, *Proc. IEEE*, *52*, 1331–1349.

Lagoutte, D., J. Cerisier, J. Plagnaud, J. Villain, and B. Forget (1992), High latitude ionospheric electrostatic disturbance studied by means of the wavelet transform, *J. Atmos. Terr. Phys.*, *54*, 1283–1294.

Lauben, D. S., U. S. Inan, T. F. Bell, and D. A. Gurnett (2002), Source characteristics of ELF/VLF chorus, *J. Geophys. Res.*, *107*(A12), 1429, doi:10.1029/2000JA003019.

LeDocq, M. J., D. A. Gurnett, and G. B. Hospodarsky (1998), Chorus source locations from VLF Poynting flux measurements with the Polar spacecraft, *Geophys. Res. Lett.*, *25*, 4063–4066.

Lefeuvre, F., and M. Parrot (1979), The use of the coherence function for the automatic recognition of chorus and hiss observed by GEOS, *J. Atmos. Terr. Phys.*, *41*, 143–152.

Lefeuvre, F., J. L. Rauch, D. Lagoutte, J. J. Berthelier, and J. C. Cerisier (1992), Propagation characteristics of dayside low-altitude hiss: Case studies, *J. Geophys. Res.*, *97*, 601–620.

Meredith, N. P., R. B. Horne, and R. R. Anderson (2001), Substorm dependence of chorus amplitudes: Implications for the acceleration of electrons to relativistic energies, *J. Geophys. Res.*, *106*, 13,165–13,178.

Meredith, N. P., M. Cain, R. B. Horne, R. M. Thorne, D. Summers, and R. R. Anderson (2003), Evidence for chorus-driven electron acceleration to relativistic energies from a survey of geomagnetically disturbed periods, *J. Geophys. Res.*, *108*(A6), 1248, doi:10.1029/2002JA009764.

Meredith, N. P., R. B. Horne, R. M. Thorne, D. Summers, and R. R. Anderson (2004), Substorm dependence of plasmaspheric hiss, *J. Geophys. Res.*, *109*, A06209, doi:10.1029/2004JA010387.

Mosier, S. R. (1971), Poynting flux studies of hiss with the Injun 5 satellite, *J. Geophys. Res.*, *76*, 1713–1728.

Mosier, S. R., and D. A. Gurnett (1969), VLF measurements of the Poynting flux along the geomagnetic field with the Injun 5 satellite, *J. Geophys. Res.*, *74*, 5675–5687.

Muzzio, J. L. R., and J. J. Angerami (1972), Ogo 4 observations of extremely low frequency hiss, *J. Geophys. Res.*, *77*, 1157–1173.

Nunn, D., Y. Omura, H. Matsumoto, I. Nagano, and S. Yagitani (1997), The numerical simulation of VLF chorus and discrete emissions observed on the Geotail satellite using a Vlasov code, *J. Geophys. Res.*, *102*, 27,083–27,097.

Parrot, M. (1990), World map of ELF/VLF emissions as observed by a low-orbiting satellite, *Ann. Geophys.*, *8*, 135–146.

Parrot, M., O. Santolík, N. Cornilleau-Wehrlin, M. Maksimovic, and C. Harvey (2003), Source location of chorus emissions observed by Cluster, *Ann. Geophys.*, *21*(2), 473–480.

Parrot, M., O. Santolík, N. Cornilleau-Wehrlin, M. Maksimovic, and C. Harvey (2004a), Magnetospherically reflected chorus waves revealed by ray tracing with Cluster data, *Ann. Geophys.*, *21*, 1111–1120.

Parrot, M., O. Santolík, D. Gurnett, J. Pickett, and N. Cornilleau-Wehrlin (2004b), Characteristics of magnetospherically reflected chorus waves observed by Cluster, *Ann. Geophys.*, *22*, 2597–2606.

Parrot, M., et al. (2006), The magnetic field experiment IMSC and its data processing onboard DEMETER: Scientific objectives, description and first results, *Planet. Space Sci.*, *54*(5), 441–455.

Rauch, J., F. Lefeuvre, J. Cerisier, J. Berthelier, N. Boudko, G. Michailova, and O. Kapustina (1985), Attenuation bands and cut off frequencies for ELF electromagnetic waves, in *CNES-Results of the ARCAD-3 Project and of the Recent Programmes in Magnetospheric and Ionospheric Physics*, p. 435, Cepadues, Toulouse, France.

Rauch, J., F. Lefeuvre, D. L. Quéau, A. Roux, J. Bosqued, and J. Berthelier (1993), Heating of proton conics by resonant absorption in a multicomponent plasma: 1. Experimental evidence, *J. Geophys. Res.*, *98*, 13,347–13,361.

Russell, C. T., R. E. Holzer, and E. J. Smith (1969), OGO 3 Observations of ELF noise in the magnetosphere: 1. Spatial extent and frequency of occurrence, *J. Geophys. Res.*, *74*, 755–777.

Santolík, O., and D. A. Gurnett (2003), Transverse dimensions of chorus in the source region, *Geophys. Res. Lett.*, *30*(2), 1031, doi:10.1029/2002GL016178.

Santolík, O., and M. Parrot (1998), Propagation analysis of electromagnetic waves between the helium and proton gyrofrequencies in the low-altitude auroral zone, *J. Geophys. Res.*, *103*, 20,469–20,480.

Santolík, O., and M. Parrot (1999), Case studies on wave propagation and polarization of ELF emissions observed by Freja around the local proton gyrofrequency, *J. Geophys. Res.*, *104*, 2459–2475.

Santolík, O., and M. Parrot (2000), Application of wave distribution function methods to an ELF hiss event at high latitudes, *J. Geophys. Res.*, *105*, 18,885–18,894.

Santolík, O., M. Parrot, L. Storey, J. Pickett, and D. A. Gurnett (2001), Propagation analysis of plasmaspheric hiss using Polar PWI measurements, *Geophys. Res. Lett.*, *28*, 1127–1130.

Santolík, O., D. A. Gurnett, J. S. Pickett, M. Parrot, and N. Cornilleau-Wehrlin (2003a), Spatio-temporal structure of storm-time chorus, *J. Geophys. Res.*, *108*(A7), 1278, doi:10.1029/2002JA009791.

Santolík, O., M. Parrot, and F. Lefeuvre (2003b), Singular value decomposition methods for wave propagation analysis, *Radio Sci.*, *38*(1), 1010, doi:10.1029/2000RS002523.

Santolík, O., D. A. Gurnett, J. S. Pickett, M. Parrot, and N. Cornilleau-Wehrlin (2004), A microscopic and nanoscopic view of storm-time chorus on 31 March 2001, *Geophys. Res. Lett.*, *31*, L02801, doi:10.1029/2003GL018757.

Santolík, O., D. A. Gurnett, J. S. Pickett, M. Parrot, and N. Cornilleau-Wehrlin (2005), Central position of the source region of storm-time chorus, *Planet. Space Sci.*, *53*, 299–305.

Shklyar, D. R., and F. Jiříček (2000), Simulation of nonducted whistler spectrograms observed aboard the Magion 4 and 5 satellites, *J. Atmos. Terr. Phys.*, *62*, 347–370.

Smith, A. J., R. B. Horne, and N. P. Meredith (2004), Ground observations of chorus following geomagnetic storms, *J. Geophys. Res.*, *109*, A02205, doi:10.1029/2003JA010204.

Solomon, J., N. Cornilleau-Wehrlin, A. Korth, and G. Kremser (1988), An experimental study of ELF/VLF hiss generation in the Earth's magnetosphere, *J. Geophys. Res.*, *93*, 1839–1847.

Storey, L. R. O. (1953), An investigation of whistling atmospherics, *Philos. Trans. R. Soc. London, Ser. A*, *246*, 113–141.

Storey, L. R. O., F. Lefeuvre, M. Parrot, L. Cairó, and R. Anderson (1991), Initial survey of the wave distribution functions for plasmaspheric hiss observed by ISEE 1, *J. Geophys. Res.*, *96*, 19,469–19,489.

Taylor, W. W. L., and D. A. Gurnett (1968), Morphology of VLF emissions observed with the Injun 3 satellite, *J. Geophys. Res.*, *73*, 5615–5626.

Thorne, R., E. Smith, R. Burton, and R. Holzer (1973), Plasmaspheric hiss, *J. Geophys. Res.*, *78*, 1581–1596.

Trakhtengerts, V. (1999), A generation mechanism for chorus emission, *Ann. Geophys.*, *17*, 95–100.

————————————

J. Chum, Institute of Atmospheric Physics, Bocni II/1401, CZ-14131 Praha 4, Czech Republic. (jch@ufa.cas.cz)

N. Cornilleau-Wehrlin, CETP/IPSL, 10/12 Avenue de L'Europe, F-78140 Velizy, France. (nicole.cornilleau@cetp.ipsl.fr)

D. A. Gurnett and J. S. Pickett, Department of Physics and Astronomy, University of Iowa, Iowa City, IA 52242-1479, USA. (donald-gurnett@uiowa.edu; pickett@uiowa.edu)

M. Parrot, LPCE/CNRS, 3A Avenue de la Recherche, Orléans, F-45071 France. (mparrot@cnrs-orleans.fr)

O. Santolík, Faculty of Mathematics and Physics, Charles University, V Holešovičkách 2, Prague, CZ-18000 Czech Republic. (ondrej.santolik@mff.cuni.cz)